Characterization of Melt-Derived 45S5 and sol-gel–derived 58S Bioactive Glasses

Pilar Sepulveda, Julian R. Jones, Larry L. Hench

Department of Materials, Centre for Tissue Regeneration and Repair, Imperial College of Science, Technology and Medicine London SW7 2BP, United Kingdom

Received 29 March 2001; revised 25 July 2001; accepted 31 July 2001

Abstract: The ability of bioactive glasses to form a bond to living bone and also to stimulate bone-cell proliferation depends on the chemical composition and on the surface texture of the glasses. In this work, the differences in physical properties between the melt-derived 45S5 and sol-gel–derived 58S Bioglass® powders of various particle-size ranges were studied. The powders were characterized for particle-size distribution by laser spectrometry, for specific surface area and porosity by nitrogen sorption analysis, and for morphological features by scanning electron microscopy. Melt-derived 45S5 powders exhibited a low-porosity texture with surface area in the range 0.15–2.7 m^2/g. In contrast, the sol-gel–derived powders exhibited a highly mesoporous texture, with surface area in the range of 126.5–164.7 m^2/g and a large fraction of 6–9 nm pore sizes. These differences in texture, as well as variations in chemical composition, account for significant changes in the resorption and *in vivo* responses.
 J Biomed Mater Res (Appl Biomater) 58: 734–740, 2001

Keywords: bioactive glasses; sol-gel; melting; particle size; nitrogen sorption

INTRODUCTION

Bioactive glasses and glass ceramics (apatite/wollastonite) have been extensively investigated for applications as bone grafts because of their ability to form a bond to living bone.[1] The glass network dissolution with the development of a silica-rich gel layer and the deposition of an apatite-like layer on the glass surface have been found to be essential steps for bonding of glass to living tissue *in vivo*.[2] *In vitro* tests involving the immersion of bioactive glasses in simulated body fluids have shown similar mechanisms of apatite layer formation as those observed *in vivo*.[2] The levels of bioactivity, that is, the rate of apatite layer formation, and the apatite-like layer thickness depend on the glass chemical composition and on the morphological parameters, such as surface area, pore size, and pore volume.[3–5]

The importance of glass textural features on levels of bioactivity grew with the advent of sol-gel–derived bioactive glasses.[5,6] Originally, bioactive glasses were prepared through melting of related oxides, at temperatures in the range of 1100–1300 °C.[1] The glass compositions were mainly based on four component systems, including silica, calcium, phosphate and sodium.[1,6] The sol-gel route enabled production of glasses with enhanced bioactivity, compared to melt-derived glasses with same composition, because of the highly porous nature of this material.[5,6] Studies have shown that sol-gel glasses prepared within three (SiO_2-CaO-P_2O_5) and two (SiO_2-CaO) component systems, and even pure silica, can quickly develop an apatite layer in contact with simulated body fluids.[7–9] Sol-gel has the advantages of low processing temperatures and ease of control of textural properties. Common precursors for silica-based sol-gel glasses include alkoxides such as tetraethylorthosilicate (TEOS) for SiO_2, triethylphosphate or phosphoric acid for P_2O_5, and salts of calcium for CaO. The fluid sol mixture undergoes hydrolysis and condensation to form a gel. The gel is then aged, dried, and thermally stabilized at temperatures that typically vary in the range of 600–800 °C.[4,5,9]

Thus, it is important to compare, with the use of the same instrumental analysis methods, the physical properties of bioactive glass powders produced through melting of the composition 45S5 with those of powders made by the sol-gel process of the 58S composition.[10–13] The two glasses are well known for their high level of bioactivity, both *in vitro* and *in vivo*. This study gives a basic description of the physical features involved in the control of dissolution behavior of the glasses and, subsequently, in the expected differences in bioactivity. The dissolution behavior and bioactivity of both types of glass were also studied and are reported on elsewhere.[14,15]

MATERIALS AND METHODS

Characterization of Bioactive Glasses

Bioactive glasses produced through melting (45S5, 46.1% SiO_2, 24.4% Na_2O, 26.9% CaO and 2.6% P_2O_5, in mol

Correspondence to: Dr. P. Sepulveda, presently at IPEN/CNEN, Divisão de Materiais Cerâmicos CCTM, Travessa R, 400 – Cidade Universitária, 05508-900, São Paulo, S. P., Brazil (e-mail: pilarsi@net.ipen.br)

Contract grant sponsor: The State of São Paulo Research Foundation (FAPESP); contract grant number: 99/02172-4

Contract grant sponsor: Engineering and Physical Sciences Research Council (ESPRC)

percent) and sol-gel processing (58S, 60% SiO_2, 36% CaO and 4% P_2O_5, in mol percent) provided by U. S. Biomaterials were investigated in this work. Three particle-size distribution ranges were tested as supplied, namely, fine (≈5–20 (μm), medium (≈90–300 (μm), and coarse (≈90–710 (μm) powders. The characterization of the powders included particle-size distribution, specific surface area, porosity, and morphological features.

The particle-size distribution of the powders was determined in aqueous medium by laser scattering analysis (Cilas Particle Sizer LD1064). The powder was sonicated and dispersed with the help of surfactants prior to the measurement.

The specific surface area and the porosity of the powders were determined by the nitrogen adsorption technique (Autosorb AS6, QuantaChrome). For these experiments, accurately measured masses of powder were submitted to evacuation and pretreatment at 100 °C for 15 h to remove moisture and contaminants. The volume of nitrogen physisorbed onto the powder surface at different relative pressures (P/P_0) was measured (nitrogen isotherms). The first seven points of the adsorption branch (relative pressures of 0.05–0.3) in the nitrogen isotherms were fitted to a BET equation to determine the specific surface area and the BET constant C, which denotes the degree of interaction between the adsorptive gas and the solid surface.[16]

Adsorption and desorption isotherm curves were also assessed to evaluate the porosity and type of porous structure of the powders. The isotherms were evaluated according to the changes in adsorption modes according to Brunauer and IUPAC classifications.[17,18] The mean pore size was calculated according to the BJH method, using the ratio between the specific pore volume (nitrogen adsorbed) and the BET surface area.[19] According to their size, pores are classified into micropores (<2 nm), mesopores (2–50 nm) and macropores (50 nm). The BJH is a method commonly applied to evaluate pore sizes in the mesoporous range. All analyses were based upon calibrations using the new mesoporous silica standard.[19]

The skeletal density was determined by automated helium displacement pycnometry (Ultrapycnometer 1000, QuantaChrome), with the use of a known mass of powder previously dried at 80 °C for 24 h. By relating the pore volume (cc/g) measured by nitrogen sorption to the true density measured by helium pycnometry, the intraparticle porosity was calculated. The tap density of the powders was obtained with help of a tapping device (Autotap, Quantachrome), by vibrating an aliquot of 10 g of powder in a 10-ml measuring cylinder and registering the final volume (~1500 taps).

Electron microscopy (JEOL, JSM T220A) was carried out to examine morphological and surface textural features of the powders.

RESULTS

Particle-Size Distribution

The curves of particle-size distribution represented in cumulative percentage and in frequency percentage as a function of the equivalent spherical particle diameter are shown in Figure 1. A summary of the results obtained from particle-size distribution measurements is also given in Table I. The values stated represent the calculated mean, mode, the equivalent spherical diameter at a cumulative percentage of 50% ($D_{50\%}$), and the particle dispersion represented here by the interpercentile range between 10% and 90%.

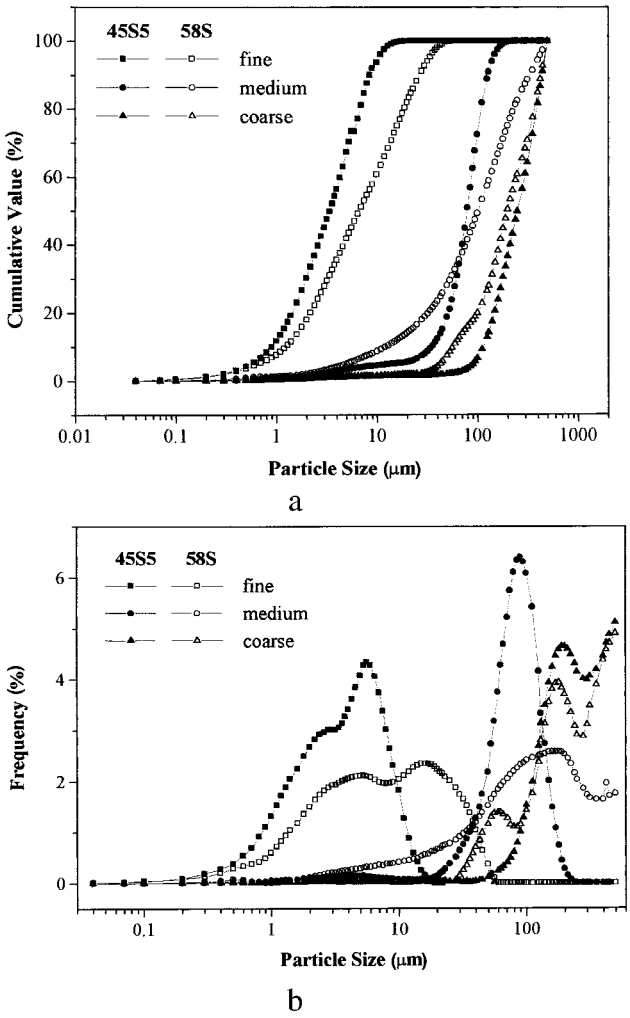

Figure 1. Curves of particle-size distribution of melt-derived 45S5 and sol-gel–derived 58S, showing the (a) cumulative percentage (%vol) and (b) frequency percentage as function of the equivalent spherical diameter.

Three different particle-size ranges were studied for the melt-derived 45S5 and three for the sol-gel–derived 58S powders, and these ranges varied widely from fractions of a micron up to a diameter greater than 500 μm (limit of the equipment). Narrow distributions characterized the powders, slightly narrower for 45S5 powders than for 58S powders. The relative frequency curves displayed more than one mode in the population data, with exception of the powder 45S5 20–90 μm, which exhibited a monomodal distribution. The $D_{50\%}$ value was used herein as the single reference value to represent the distribution of particle size, rather than the mean, because it takes into account the frequency distribution. For 45S5 fine, medium and coarse powders, $D_{50\%}$ of 3.4, 79.2, 223.6 μm were measured and for 58S, $D_{50\%}$ of 6.7,

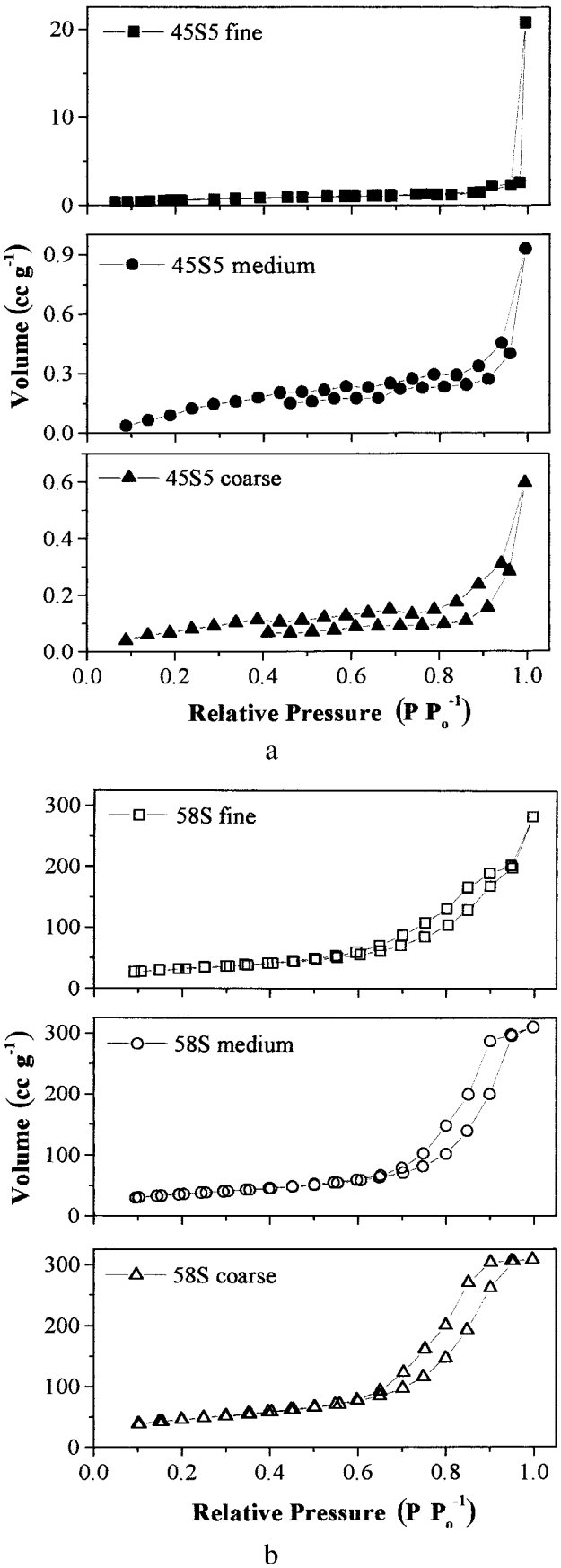

Figure 2. Nitrogen sorption isotherms for (a) melt-derived 45S5 and (b) sol-gel–derived 58S powders.

102.2, 198.2 μm, respectively. The medium and coarse distributions overlapped slightly.

BET Surface Area

Data of surface analysis obtained by nitrogen adsorption are listed in Tables II and Table III. The specific surface area for the 45S5 powders measured by the BET method was very low, decreasing from 2.7 to 0.15 m^2g^{-1} as the particle size increased from 3.4 μm (fine powder) to 223.6 μm (coarse powder). Much higher specific surface area was measured for sol-gel–derived 58S powders, ranging from 126.5 to 164.7 m^2g^{-1} for similar ranges of particle size, with corresponding $D_{50\%}$ values of 6.7 (fine powder) to 198.2 μm (coarse powder). No apparent relation of specific surface area with particle size was found in this case. The melt-derived 45S5 powders displayed a very low adsorption BET constant C ranging from 30.0 to 31.4. In contrast, the sol-gel–derived 58S powders exhibited a high adsorption constant on BET analysis (157.8–243.0). Large C values are associated with strong interactions between the adsorptive gas and the solid surface.

Nitrogen Isotherms

More detailed analysis of porous texture was revealed by the nitrogen sorption isotherms. Most isotherms can be classified by shape into one of six types (I–VI) according to the changes in adsorption modes, as described by Brunauer and IUPAC.[17,18] For instance, Type I (rapid rise in the amount of adsorption at increasing pressure up to a limiting value) represents monolayer coverage in microporous solids. Type II (S-shaped or sigmoidal) indicates monolayer–multilayer formation in nonporous or macroporous materials. Type IV (level off near the saturation vapor pressure) occurs for mesoporous materials.[17,18]The isotherm curves measured for the bioactive powders in this work are shown in Figures 2(a) and 2(b), for 45S5 and 58S powders, respectively. The melt-derived 45S5 powders displayed a very low adsorption, mainly monolayer formation followed by saturation, revealing negligible levels of porosity. In contrast, the sol-gel–derived 58S powders exhibited a Type IV isotherm and multilayer formation, which is the result of surface coverage of pore walls in the mesoporous range followed by pore filling. The hysteresis loops in adsorption-desorption modes are commonly attributed to the presence of cylindrical pores.[18]

Pore-Size Distribution

Table II gives a summary of mean pore size measured by the BJH method. The sol-gel–derived powders contained mainly mesopores within the range of 6.5–9.5 nm. The porous nature of these materials originates from the manner by which the gel is formed. The alkoxide precursors react readily with water, and the hydrolyzed species link together in a condensation reaction that can form a three-dimensional polymeric network, because the monomer is tetrafunctional [$Si(OH)_4$]. The liquid solvents that participate in the process are retained in the capillaries of the structure and, after drying, a solid network with continuous porosity results. The pores may vary

TABLE I. Data of Powder Characterization: Mean of Particle Size Distribution (ϕ_{mean}), Equivalent Spherical Diameter at the Cumulative Volume Percentage of 50% ($D_{50\%}$); Diameter Range Considered Here as $D_{10\%}$–$D_{90\%}$, Measured by Laser Spectrometry

Sample	Description	Modes	ϕ_{mean} (μm)	$D_{50\%}$ (μm)	$D_{10\%–90\%}$ (μm)
I	45S5 fine	2.8/5.6	4.0	3.4	0.9–8.0
II	45S5 medium	3.8/90	80.5	79.2	35.0–127.8
III	45S5 coarse	200/>500	248.1	223.6	107.6–434.7
IV	58S fine	5/16	10.8	6.7	1.2–26.8
V	58S medium	170/>500	138.7	102.2	12.2–334.4
VI	58S coarse	60/180/>500	227.0	198.2	57.2–432.6

in size and may be interconnected or completely closed, depending on the processing conditions and stabilization temperature.[20]

Melt-derived powders, on the other hand, contained very little porosity and almost negligible adsorption levels. Although the pore-size measurements (1.6–2.1 nm) are not very precise at such low adsorption levels, they lie within the size scale of glass surface roughness. Surface roughness of particles produced from melt-derived glasses has been associated with surface tension of the melt (melt-formed surfaces) and with intrinsic heterogeneities in glass structure (fracture surfaces).[21]

Density

The results of skeletal density, tap density, and intraparticle porosity are given in Table III. The skeletal density of the powders measured by helium pycnometry varied within the range of 2.71–2.82 g cm^{-3}, independent of particle size or composition. The total porosity in the 45S5 fine, medium, and coarse powders was 8.94%, 0.47%, and 0.29%, respectively, compared to 37–57% for the 58S powders.

In tap density experiments, sol-gel–derived powders packed with a density of 0.63–0.69 g cm^{-3}, independent of the particle size. Conversely, the finest 45S5 powder packed with a density of 0.80 g cm^{-3}, whereas the medium and coarse 45S5 powders packed at much higher density of 1.18 and 1.33 g cm^{-3}, respectively. In spite of the simplicity of tap density tests, a useful comparative measurement is obtained that can indicate the packing ability and fluidity of the powders. The low packing density and fluidity of the 58S powders is related to the high intraparticle porosity and increased surface roughness that is be associated with the processing method.

Microstructural Features

The texture of the melt-derived 45S5 powders is illustrated in Figures 3(a)–3(c), for coarse, medium, and fine powders, respectively. The particles appear to have angular, irregular, nonspherical shapes, as is typical for products of grinding processes. The size of particles observed from the SEM micrographs was of same magnitude as the laser scattering particle-size data. The finest powders appeared to form agglomerates as a result of weak-attraction van der Waals forces [Figure 3(c)]. Figure 3(d) shows the 45S5 glass surface at higher magnification, where a smooth and compact surface texture can be observed, with small defects.

The microstructural features of coarse, medium, and fine 58S powders are illustrated in Figures 4(a)–4(c). The particle shape was similar to that of 45S5 powders; however, at higher magnification the surface of 58S particles exhibited a very porous and rough texture with pores in the submicrometer range, which agreed with the surface analysis results [Figure 4(d)].

DISCUSSION

The objective of this study was to identify the differences in physical properties between melt-derived 45S5 and sol-gel–derived 58S powders—differences that are known to influence the glass dissolution and subsequent mechanisms leading to hydroxycarbonate layer formation. Many *in vivo* studies using bioactive materials to fill bone defects have demonstrated that the rate of formation of biological apatite on the surface of these materials controls the bone ingrowth rate and the rate of new bone formation.[2,10,12,22,23] Therefore, achieving a control of the reactions involved in apatite layer

TABLE II. Data of Powder Characterization: Specific Surface Area (SA), BET Constant (*C*), Mean BJH Desorption Pore Size and Pore Volume Obtained by Nitrogen Adsorption Technique

Sample	Description	SA (m^2 g^{-1})	*C*	Pore Size (Å)	Pore Volume (cc/g)
I	45S5 fine	2.70	31.4	18.8	0.0348
II	45S5 medium	0.24	30.7	21.3	0.0017
III	45S5 coarse	0.15	30.0	16.3	0.0011
IV	58S fine	126.54	192.0	65.5	0.4474
V	58S medium	128.86	243.0	95.4	0.4984
VI	58S coarse	164.73	157.8	78.7	0.2131

TABLE III. Data of Skeletal Density, Tap Density, and Calculated Intraparticle Pore Volume

Sample	Description	Skeletal Density (g cm^{-3})	Intraparticle Porosity (%-vol)	Tap Density (g cm^{-3})
I	45S5 fine	2.825	8.94	0.80
II	45S5 medium	2.744	0.47	1.18
III	45S5 coarse	2.717	0.29	1.33
IV	58S fine	2.727	54.94	0.63
V	58S medium	2.718	57.53	0.69
VI	58S coarse	2.796	37.31	0.69

Standard error. Skeletal density ± 0.002–0.009.

formation is of great importance to optimize the bone-healing process. Also, *in vitro* and *in vivo* studies involving melt-derived 45S5 and sol-gel–derived 58S glasses have accredited the much higher degradability rate and much faster formation of apatite layer of 58S glasses to the differences in texture.[11–14] However, these differences have not previously been quantified using the same analytical procedures.

In the present work, it has been shown that the melt-derived 45S5 glass particles exhibit mainly nonporous surfaces with low intrinsic roughness and low surface area, dependent on the degree of grinding. Because of the lack of textural variation produced through melting, the melt-derived glasses have shown a dissolution behavior that can be directly correlated to their chemical composition.[1,2] Therefore, for melt-derived powders, the change in particle-size range caused by different grinding periods could provide an efficient way to control dissolution rates. Finer powders exhibit higher specific surface areas; therefore, they provide more exposed surface for dissolution. Consequently, increasing deposition rates of Ca-P layer on the glass surface and the processes of material degradation and resorption have shown to occur earlier for finer powders, as demonstrated through *in vitro*[14,15] and *in vivo* studies.[10,12,22,23] Variations in texture have shown to be more important in determining the dissolution and bioactive behavior of sol-gel–derived glasses than in the melt-derived glasses.[4,5,9] The sol-gel–glass texture is highly porous; thus it promotes a higher degree of hydroxylation of the surface forming SiOH (silica-rich gel layer) than

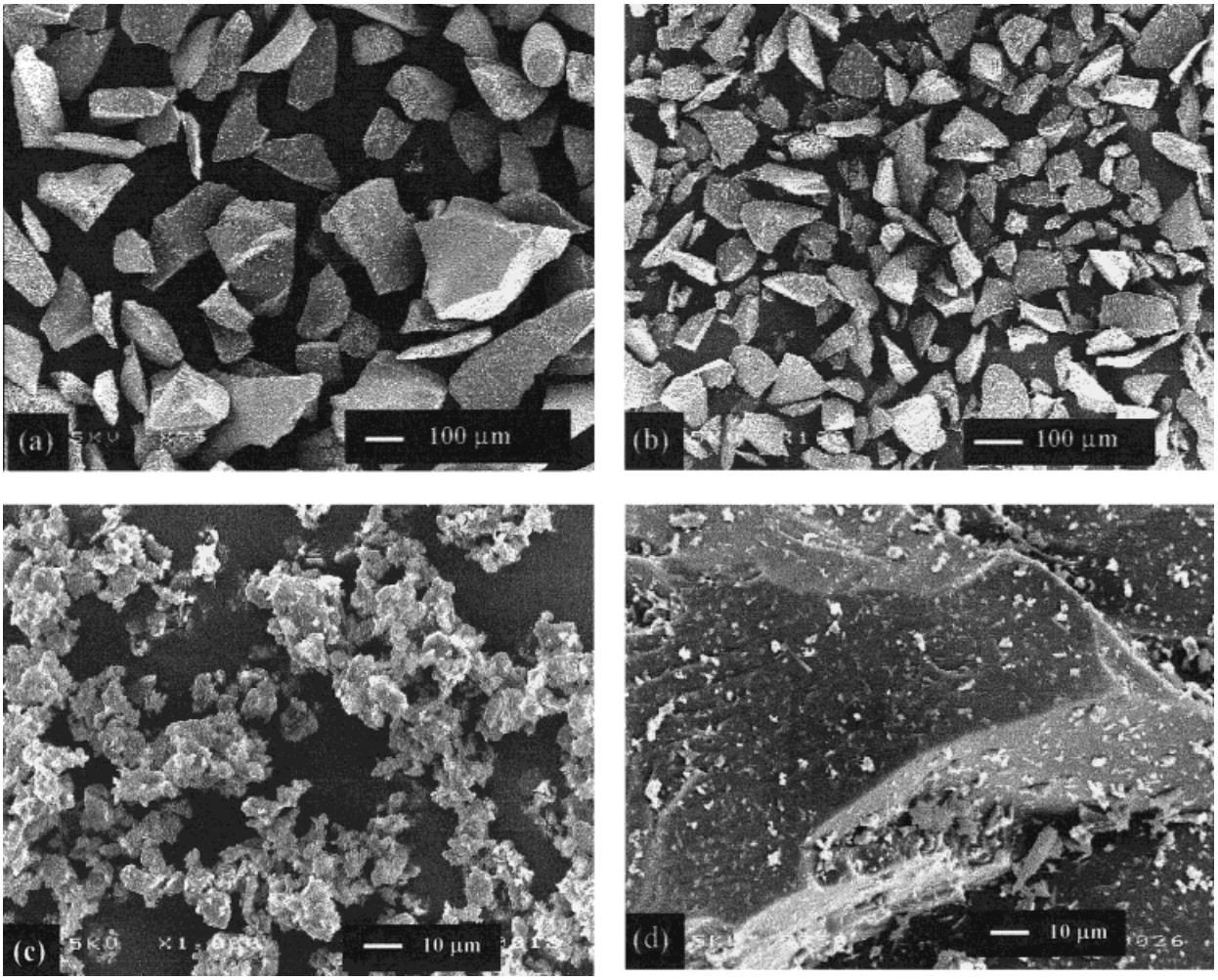

Figure 3. Illustration of the surface texture under SEM observation, for coarse (a), medium (b) and fine (c) 45S5 powders. Micrograph at higher magnification of the surface of 45S5 (d), showing nonporous surfaces with intrinsic roughness of fracture.

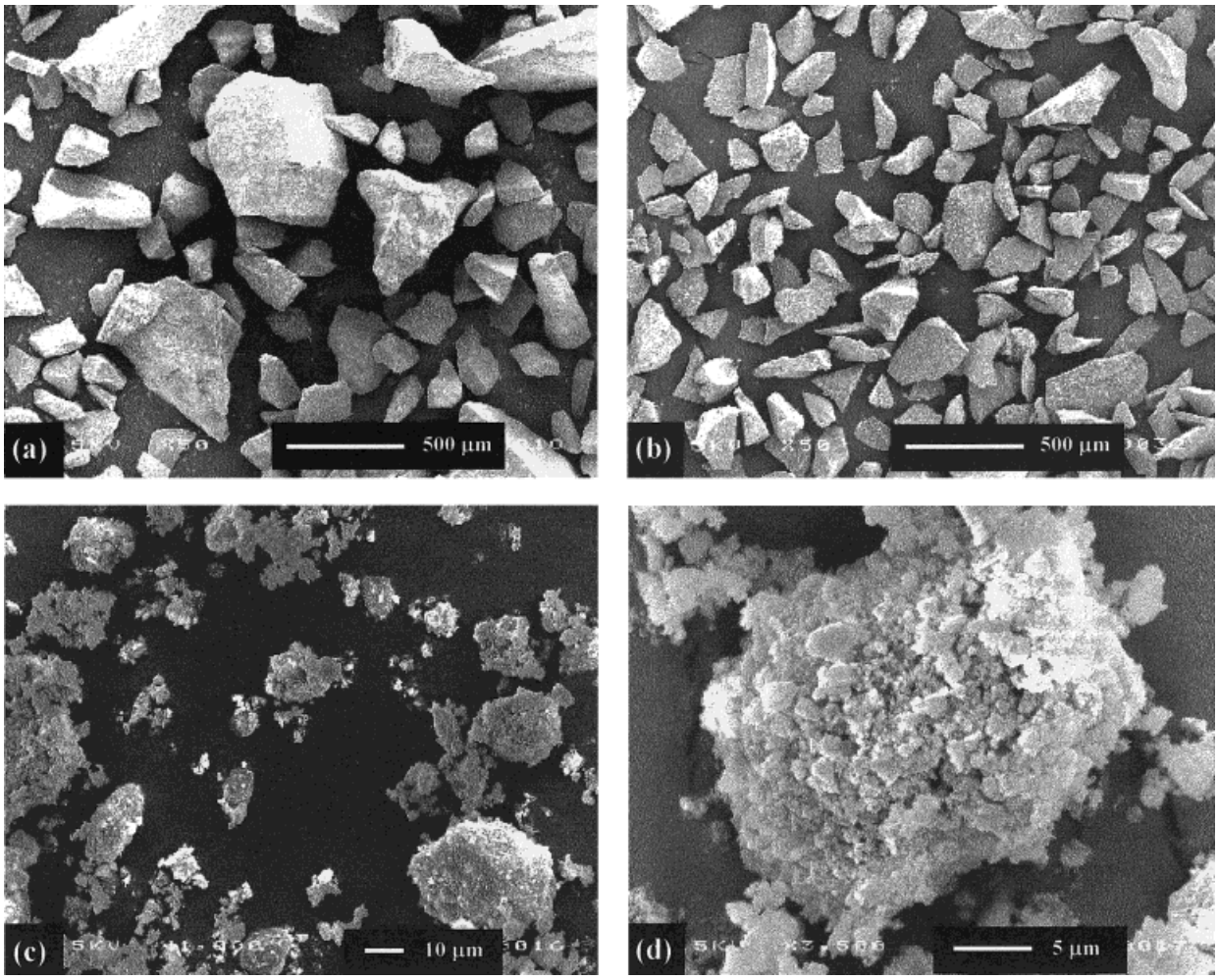

Figure 4. Illustration of the surface texture under SEM observation for (a) coarse, (b) medium, and (c) fine 58S powders. (d) Micrograph at higher magnification of 58S powders, showing the porous nature of the sol-gel–derived material.

in the 45S5 melt-derived glasses. For sol-gel–derived materials the silica-rich gel layer provides more sites for calcium-phosphate– (apatite precursor) layer nucleation.[8] Different textures can be promoted in sol-gel–derived material by simply altering specific processing parameters, such as pH, reagent concentrations, and drying and stabilization conditions. Furthermore, the large porosity of sol-gel–derived powders decreases their ability to be compacted into a fixed volume, which implies that a small mass of material is necessary to fill a void. This favors applications where faster resorption *in vivo* is needed. Because of its mesoporous texture and high surface area, which can adsorb a range of substances such as proteins and cells, the sol-gel method has become an alternative for preparing glasses for a number of applications in the biomedical field.[24]

In addition to surface texture and particle size, many other characteristics account for *in vivo* bioactivity and bone-filling ability of bioactive powders. The composition of the powder is the most important factor; glasses for the dental field, middle—ear procedures, and vertebral surgery have been fabricated within a wide compositional range in the system SiO_2-CaO-P_2O_5-Na_2O with different degrees of reactivity.[2,25] Variations in the mineralogical structure, such as the partial crystallization of melt-derived glasses (glass ceramics) have been reported as another alternative to produce tougher materials and also to control dissolution rates and bioactivity.[26] Bioactive materials such as calcium phosphate cements can have their reactivity controlled by combining phases of different solubility[27,28] or phases that react to form natural hydroxyapatite *in situ*.[29] The incorporation of interconnected macroporosity within the structure of bioactive materials has been another common approach to produce bioactive scaffolds for tissue regeneration with control of the dissolution rates.[30–33] Such a structure has the potential for vascularization and complete penetration of osseous tissue throughout the repair site.

CONCLUSIONS

The physical features of bioactive glasses typically applied in bone repair and regeneration have been investigated in this work, using two very distinct types of powder produced by the melting and by sol-gel route. These were the melt-derived

45S5 and sol-gel–derived 58S powders, which are known for their bone-regeneration features. Melt-derived 45S5 powders displayed low porosity surfaces and smooth textures, with specific surface area within 0.15 to 2.7 m^2/g. Sol-gel–derived powders, on the other hand, exhibited intrinsically higher surface areas of 126.5–164.7 m^2/g, and a high level of porosity in the mesoporous range. Variation of particle size has more influence on the physical properties of the 45S5 melt-derived glasses than on the 58S sol-gel–derived glasses. These differences have been shown in previous works to account for higher bioactivity and osteogenic potential of sol-gel–derived materials. The textural differences between the 45S5 and 58S glasses serve to illustrate the importance in understanding the material properties in order to predict their biological performance.

The authors are grateful to U. S. Biomaterials for supply of the materials.

REFERENCES

1. Hench LL, Wilson J. An introduction to ceramics. Singapore: World Scientific; 1993.
2. Hench LL, West JK. Biological applications of bioactive glasses. Life Chem Rep 1996;13:187–241.
3. Greespan DC, Zhong JP, La Torre GP. Effect of surface area to volume ratio on in vitro surface reactions of bioactive glass particles. In: Anderson OH, Yli-Urpo A, editors. Bioceramics. London: Butterworth-Heinemann; 1994. vol 7, pp 28–33.
4. Li R, Clark AE, Hench LL. Effects of structure and surface area on bioactive powders by sol-gel process. In: Hench LL, West JK, editors. Chemical processing of advanced materials. New York: John Wiley & Sons, Inc.; 1992. pp 627–633.
5. Pereira MM, Clark AE, Hench LL. Effect of texture on the rate of hydroxyapatite formation on gel-silica surface. J Am Ceram Soc 1995;78:2463–2468.
6. Filgueiras MR, LaTorre GP, Hench LL. Solution effects on the surface reactions of a bioactive glass. J Biomed Mater Res 1993;27:445–453.
7. Peltola T, Jokinen M, Rahiala H, Levanen E, Rosenholm JB, Kangasniemi I, Yli-Urpo A. Calcium phosphate formation on porous sol-gel-derived SiO_2 and $CaO\text{-}P_2O_5\text{-}SiO_2$ substrates in vitro. J Biomed Mater Res 1999;44:12–21.
8. Pereira MM, Hench LL. Mechanisms of hydroxyapatite formation on porous gel-silica substrates. J Sol-Gel Sci Technol 1996;7:59–68.
9. Li R, Clark AE, Hench LL. An investigation of bioactive glass powders by sol-gel processing. J Appl Biomater 1991;2:231–239.
10. Oonishi H, Hench LL, Wilson J, Sugihara F, Tsuji E, Kushitani S, Iwaki H. Comparative bone growth behavior in granules of bioceramic materials of various sizes. J Biomed Mater Res 1999;44:31–43.
11. Greenspan DC, Zhong JP, Chen XF, La Torre GP. The evaluation of degradability of melt and sol-gel derived Bioglass® in vitro. In: Sedel L, Rey C, eds. Bioceramics. . Zurich: Trans-Tech; 1997. pp 391–394.
12. Wheeler DL, Stokes KE, Hoellrich RG, Chamberland DL, McLoughlin SW. Effect of bioactive glass particle size on osseous regeneration of cancellous defects. J Biomed Mater Res 1998;41:527–533.
13. Hench LL, Wheeler DL, Greenspan DC. Molecular control of bioactivity in sol-gel glasses. J Sol-Gel Sci Technol1998;13: 245–250.
14. Sepulveda P, Jones JR, Hench LL. Effect of particle size Bioglass® dissolution. Bioceramics. Zurich: Trans-Tech; 2001. vol 13, pp 192–195, 629–634.
15. Sepulveda P, Jones JR, Hench LL. *In vitro* dissolution of melt-derived 45S5 and sol-gel–derived 58S bioactive glasses. J Biomed Mater Res; in press.
16. Brunauer S, Emmett PH, Teller E. Adsorption of gases in multimolecular layers. J Am Chem Soc 1938;60:309–319.
17. Sing KSW, Everett DH, Haul RAW, Moscou L, Rouquérrol RA, Rouquérrol J, Siemiewska T. Reporting physisorption data for gas/solid systems. Pure Appl Chem 1985;57:603–619.
18. Brunauer S, Deming LS, Deming WS, Teller E. On a theory of the Van der Waals adsorption of gases. J Am Chem Soc 1940; 62:1723–1732.
19. Coleman NJ, Hench LL. A gel-derived mesoporous silica references materials for surface analysis by gas sorption, part 1—Textural features. Ceram Int 2000;26:171–178.
20. Brinker CJ, Scherer GW. Sol-gel science—The physics and chemistry of sol-gel processing. London: Academic; 1990.
21. Gupta PK, Innis D, Kurkjian CR, Zhong Q. Nanoscale roughness of oxide glass surfaces. J Non-Cryst Solids 2000;262:200–206.
22. Ohgushi H, Okumura M, Yoshikawa M, Inoue K, Senpuku K, Tamai S. Bone formation process in porous calcium carbonate and hydroxyapatite. J Biomed Mat Res 1992;26:885–896.
23. Gauthier O, Bouler JM, Weiss P, Bosco J, Aguado E, Daculsi G. Short-term effects of mineral particle sizes on cellular degradation activity after implantation of injectable calcium phosphate biomaterials and the consequences for bone substitution. Bone 1999;25:71–74.
24. Hench LL. Sol-gel materials for bioceramic applications. Curr Opinion Solid State & Mater Sci 1997;2:604–610.
25. Kokubo T. A/W Glass ceramic: Processing and properties. In Hench LL, Wilson J, editors: An introduction to ceramics. Singapore: World Scientific; 1993.
26. Peitl O, La Torre GP, Hench LL. Effect of crystallization on apatite-layer formation of bioactive glass 45S5. J Biomed Mater Res 1996;30:509–514.
27. Takagi S, Chow LC, Markovic M, Friedman CD, Costantino PD. Morphological and phase characterizations of retrieved calcium phosphate cement implants. J Biomed Mater Res 2001; 58:36–41.
28. Constantz BR, Barr BM, Ison IC, Fulmer MT, Baker J, McKinney LA, Goodman SB, Gunasekaren S, Delaney DC, Ross J, Poser RD. Histological, chemical, and crystallographic analysis of four calcium phosphate cements in different rabbit osseous sites. J Biomed Mater Res 1998;43:451–461.
29. Constantz BR, Ison IC, Fulmer MT, Poser RD, Smith ST, Vanwagoner M, Ross J, Goldstein SA, Jupiter JB, Rosenthal DI. Skeletal repair by in-situ formation of the mineral phase of bone. Science 1995;267:1796–1799.
30. Markovic M, Takagi S, Chow LC. Formation of macropores in calcium phosphate cements through the use of mannitol crystals. Key Eng Mater 2000;192-1:773–776.
31. Shors EC, White EW, Kopchok G. Biocompatibility, osteoconduction and biodegradation of porous hydroxyapatite, tricalcium phosphate, sintered hydroxyapatite and calcium carbonate in rabbit bone defects. Mater Res Soc 1989;110: 211–217.
32. Sepulveda P, Binner JPG, Rogero SO, Higa OZ; Bressiani JC. Production of porous hydroxyapatite by the gelcasting of foams and cytotoxic evaluation. J Biomed Mater Res 2000;50:27–34.
33. Sepulveda P, Jones JR, Hench LL. Bioactive sol-gel foams for tissue repair. J Biomed Mater Res; in press.